



LUND UNIVERSITY

Compex: a cubic germanium detector

Sâmark-Roth, A.; Cox, D. M.; Eberth, J.; Golubev, P.; Rudolph, D.; Sarmiento, L. G.; Tocabens, G.; Ginsz, M.; Pirard, B.; Quirin, P.

Published in:

European Physical Journal A. Hadrons and Nuclei

DOI:

[10.1140/epja/s10050-020-00155-3](https://doi.org/10.1140/epja/s10050-020-00155-3)

2020

Document Version:

Peer reviewed version (aka post-print)

[Link to publication](#)

Citation for published version (APA):

Sâmark-Roth, A., Cox, D. M., Eberth, J., Golubev, P., Rudolph, D., Sarmiento, L. G., Tocabens, G., Ginsz, M., Pirard, B., & Quirin, P. (2020). Compex: a cubic germanium detector. *European Physical Journal A. Hadrons and Nuclei*, 56(5), Article 141. <https://doi.org/10.1140/epja/s10050-020-00155-3>

Total number of authors:

10

Creative Commons License:

CC BY

General rights

Unless other specific re-use rights are stated the following general rights apply:

Copyright and moral rights for the publications made accessible in the public portal are retained by the authors and/or other copyright owners and it is a condition of accessing publications that users recognise and abide by the legal requirements associated with these rights.

- Users may download and print one copy of any publication from the public portal for the purpose of private study or research.
- You may not further distribute the material or use it for any profit-making activity or commercial gain
- You may freely distribute the URL identifying the publication in the public portal

Read more about Creative commons licenses: <https://creativecommons.org/licenses/>

Take down policy

If you believe that this document breaches copyright please contact us providing details, and we will remove access to the work immediately and investigate your claim.

LUND UNIVERSITY

PO Box 117
221 00 Lund
+46 46-222 00 00

Compex - a cubic germanium detector

A. S amark-Roth^{1,a}, D.M. Cox¹, J. Eberth², P. Golubev¹, D. Rudolph¹,
L.G. Sarmiento¹, G. Tocabens^{1,b}, M. Ginzsz³, B. Pirard³, P. Quirin³

¹Department of Physics, Lund University, SE-22100 Lund, Sweden

²Institut f ur Kernphysik, Universit at zu K oln, D-50937 Cologne, Germany

³Mirion Technologies (Canberra), Lingolsheim Facility, F-67380 Lingolsheim, France

Received: date / Accepted: date

Abstract The Compex detector is an electrically cooled, composite germanium detector that uses four coaxial, cubic-shaped, single-encapsulated germanium crystals. This novel detector allows for new heights in photon detection efficiency in decay spectroscopy setups using box-shaped vacuum chambers. Its spectroscopic performance and detection efficiency is evaluated by means of source measurements. Motivated by Compex's unique cubic germanium crystals, the Lund scanning system has been developed. The constructed system is used to characterise the response as a function of interaction position within a Compex crystal. Sensitivity across the front face, pulse shapes, and rise times have been analysed. Future development and applications of the Compex detector are discussed.

1 Introduction

Ever since the first germanium detector saw its first γ ray in the mid 1960s, they have played a major role in unravelling the intrinsic structure of atomic nuclei, due to their excellent ability to resolve γ -ray energies. In the early 1990s, motivated by in-beam experiments, where γ rays are emitted in-flight, a new generation of multi-detector arrays aiming to cover a solid angle of 4π were under design. To achieve this, large volume n-type crystals were required. However, the production was mainly limited by the yield of growing sufficiently pure crystals. In light of this problem, a new concept in γ -ray spectrometry emerged; the composite germanium detector [1,2].

In these composite detectors, several crystals are assembled in a common cryostat. To this day, mainly two types of composite detectors have been produced, Clover type [2,3] and Cluster type [4] detectors. These comprise four and seven crystals, respectively. A new technique of single-crystal encapsulation was introduced with the Cluster detector. The seven crystals were each hermetically sealed at high vacuum in an aluminium canister, increasing the reliability of the composite detector while maintaining a very compact geometry [5]. Clover and Cluster detectors formed parts of the EUROBALL [6] and the EUROGAM [7] arrays together with Bismuth-Germanate (BGO) escape suppression shields. In these arrays, the composite detectors allowed for larger germanium volumes and thus higher full-energy peak efficiency compared to the preceding monolithic detectors as well as smaller Doppler broadening and better Doppler shift corrections due to a considerable increase in granularity.

Following these arrays of composite detectors, the first 4π γ -ray spectrometers without escape suppression were on the drawing boards in the late 1990s. The keys to the realisation of these large arrays were three-fold. Firstly, the development of hexagonal-tapered germanium crystals, which despite distorted electric fields, showed excellent spectral properties [4]. Secondly, position sensitive, segmented detectors eliminating the need for the escape suppression. Thirdly, the encapsulation technology which enabled compact geometries of highly-segmented detectors in a common cryostat. By using γ -ray tracking, the contemporary 4π γ -ray spectrometers, AGATA [8] and GRETA [9] presently lead the way for sensitivity and count-rate capabilities while maintaining high spectral qualities using spherical target chambers for in-beam experiments.

^ae-mail: anton.samark-roth@nuclear.lu.se

^bCurrent address: Universit e Paris-Saclay, CNRS/IN2P3, IJCLab, F-91405 Orsay, France

As the development of AGATA and GRETA were starting, other spectrometers, *e.g.* the EUROBALL and EUROGAM arrays, ended their campaigns. Some of the detectors of these arrays instead saw a use in decay spectroscopy setups, typically located at the focal plane of recoil separators, fragment separators, or the like. In decay spectroscopy, structural properties of a radioactive nucleus, selected by the separator, are investigated by measuring the energy spectra of emitted charged particles in an array of silicon detectors and photons in surrounding germanium detectors. TASI-Spec [10] is one of these setups which employed EUROGAM-type Clover and EUROBALL Cluster detectors. To ensure highest detection efficiency, the germanium detectors are packed as close as possible to the silicon detectors with as little material as possible between. Many successful experiments have been conducted with this technique. For instance, precise spectroscopy with TASI-Spec allowed the first derivation of excitation schemes of isotopes along decay chains starting with superheavy element $Z = 115$, moscovium [11].

In contrast to AGATA and GRETA with their spherical target chambers surrounding primary or secondary in-beam target foils, the decay spectroscopy setups typically have box-shaped vacuum chambers due to constraints caused by the silicon detector arrangement. Here, the coaxial cylindrical or hexagonal-tapered shapes and long end-cap to germanium crystal distances in the existing germanium detectors lead to a sub-optimal detection efficiency. In order to further push down the observational limit and increase sensitivity, the solid angle coverage can be improved with rectangular shaped germanium crystals in compact capsules. The development of encapsulation, the properties of hexagonal tapered detectors and pulse shapes as function of the field strength studied with segmented detectors [12, 13] has now led to the construction of *Compex*. *Compex*, being a portmanteau of compact and exotic, is the first γ -ray detector using coaxial, cubic-shaped, germanium crystals.

In this paper, the *Compex* detector is introduced in detail in Sect. 2. Hereafter, a thorough characterisation of the detector is given; Source measurements demonstrating spectral properties including energy resolution and full-energy peak detection efficiency, are described in Sect. 3. A description of the *Lund Scanning System* initiates Sect. 4, it is employed in two measurements. In a front-face scan, the geometry and sensitivity across the front face is probed in detail. Thereafter, the pulse shape response of the detector as a function of interaction position (x, y, z) is characterised in a coincidence scan. Additionally, distributions of rise times at three different energies are analysed for a general pulse shape

characterisation. Finally, conclusions and an outlook for the use of the *Compex* detectors are presented in Sect. 5.

2 The *Compex* germanium detector

The *Compex* detector is a composite germanium detector manufactured by *Mirion Technologies (Canberra)*. It comprises four coaxial, cubic-shaped, $50 \times 50 \times 50 \text{ mm}^3$ single-encapsulated germanium crystals mounted in a common cryostat with an aluminium end-cap. The compactness of *Compex* is indicated in a schematic drawing of the end-cap from the side face in Fig. 1(a). The crystals are n-type with boron implanted p^+ and Li diffused n^+ contacts. The n^+ contact is a bore hole on the pure side of the crystals. The fast crystallographic axis, $\langle 100 \rangle$, is aligned with the diagonals, while the slower $\langle 110 \rangle$ axis is perpendicular to the sides of the crystal as illustrated in Fig. 1(b) where the detector is shown without its end-cap.

A positive high voltage is applied to the core contact. The nominal depletion voltage is 2500 V and the detector is operated at 3500 V. The signals generated at the core contact are readout through AC-coupling with resistive charge sensitive preamplifiers, PSC 763 manufactured by *Mirion Technologies (Canberra)*. The energy output signal has a sensitivity of 350 mV/MeV when loaded with 1 M Ω , a DC offset of less than ± 10 mV and a decay constant of 50 μs . The detector module is equipped with a housing for preamplifiers, and feed-throughs for; HV supplies, preamplifier power supply, PT100 temperature readout, bias shutdown and two energy plus one time output signals for each crystals via SMA connectors (see Fig. 2(a)).

The detector is cooled with an electrically refrigerated cryostat, *Cryo-Pulse[®] 5 plus* [14], located at the right in the side view of the detector in Fig. 2(a). In steady-state operating conditions the electrical power consumption of a *Compex* detector is typically around 120 W, while the germanium crystal temperature is -160°C , *i.e.* significantly above liquid nitrogen temperature. However, settings of the cryo-cooler can be modified such that the detector can be operated at a desired temperature optimised for *e.g.* minimising electron trapping. The cryostat is equipped with heating elements, such that outgassing/annealing can be readily performed via service and pumping ports.

The detection head is offset with respect to the center of the rest of the module. This and the geometry of the cryo-cooler makes it possible to tessellate four *Compex* detectors into a *wall* configuration, as depicted in Fig. 2(b). From the aluminium end-cap, a stainless steel cylinder leads to a flange. The flange enables the

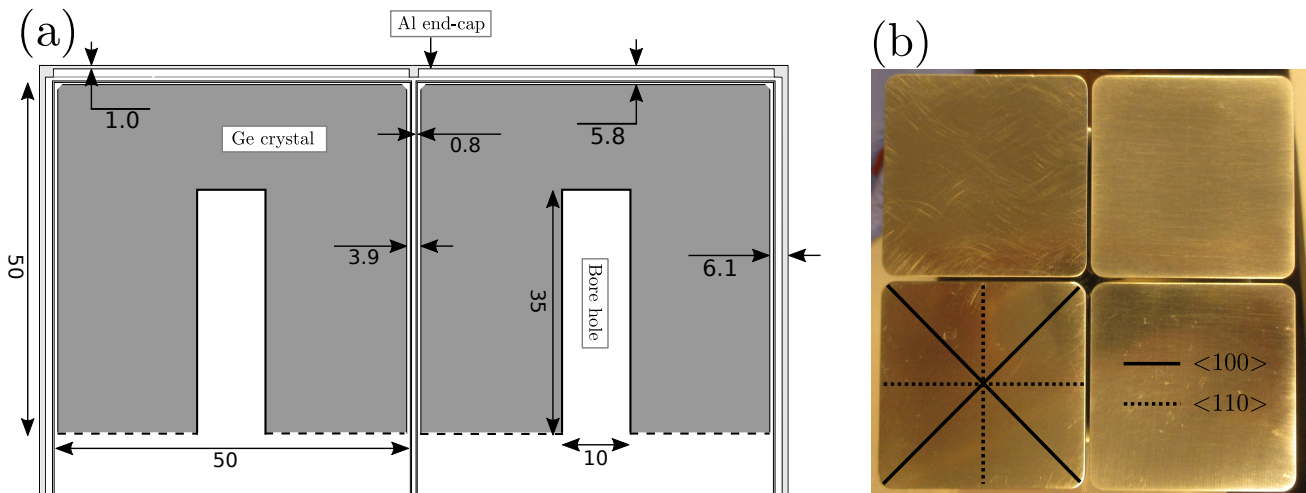


Fig. 1: (a) Schematic drawing of the Complex germanium crystals, individual capsules and end-cap from the side face including measurements (mm). (b) Complex detector without end-cap where crystallographic axes are indicated. See text for details.

mounting of the detector to a vacuum chamber. Within a vacuum chamber, the detector may be operated without the end-cap to increase detection efficiency of low energy γ and X rays.

3 Source measurements

The spectroscopic performance of all the crystals in the four Complex detectors has been evaluated in factory acceptance tests performed at the *Mirion Technologies (Canberra)* Lingolsheim facility. In these measurements, a ^{60}Co source was placed in a holder such that it was centred with respect to the Complex detector and gave a count rate of $\sim 1000/\text{s}$ per crystal. Analogue measurements were made with a readout through Canberra 2026 spectroscopy amplifiers, and an analogue to digital converter and multichannel analyser Canberra Multiport II unit. The pole-zero compensated amplifier signal had a $4\ \mu\text{s}$ shaping time and a gain which placed the 1332 keV peak in the middle of the dynamic range of the 16K ADC.

The average crystal performances in these measurements, obtained with the acquisition software *Genie 2k* [15], are compiled in Table 1(a). The energy resolutions at 60 and 122 keV were obtained with a ^{241}Am and a ^{57}Co source, respectively. The resolution together with the peak shapes demonstrate Complex's great spectroscopic performance. Much due to the low capacitance of 28 pF, the resolution obtained at low energy is in general better than other Clover detectors, *e.g.* the EURO-GAM II [2] with 1.03(2) keV at 122 keV while at 1332 keV it is comparable. The peak-to-Compton ratio has been defined as the ratio of the average chan-

nel height in the ^{60}Co energy spectrum in the range [1040, 1096] keV and the maximum number of counts per channel in the 1332 keV peak.

Table 1: (a) Average spectroscopic performance of all the crystals in four Complex detectors as obtained in the factory acceptance tests. The uncertainties given here have been calculated as the standard deviation from the mean. (b) Relative efficiencies at 1332 keV for the different detection modes, see Sect. 3.2.

(a)	
FWHM at 60 keV	0.72(4) keV
FWHM at 122 keV	0.80(4) keV
FWHM at 1332 keV	1.94(14) keV
FWTM/FWHM	1.92(9)
FWFM/FWHM	2.65(20)
Peak-to-Compton ratio	49(4)%
(b)	
Direct mode	30.8(4)%
Total mode	123.0(17)%
Add-back mode	161.1(21)%

Further source measurements were undertaken in Lund to determine the energy resolution and the full-energy peak efficiency as functions of energy. The readout was performed with a VME compatible *Struck SIS3302* 16 bit 100 MHz digitiser module. The energy spectra were obtained with an FPGA trapezoidal routine with correction for the exponential decay of the preamplifier signal. The averaging width was set to $6.4\ \mu\text{s}$, and the gap to $1.2\ \mu\text{s}$, corresponding to the rise time of the

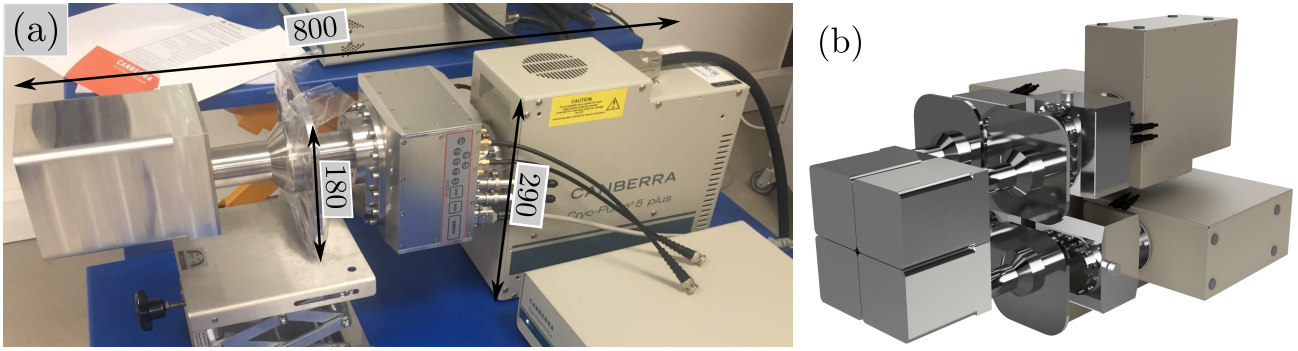


Fig. 2: **(a)** Complex detector module. From left to right; aluminium end-cap, flange, housing of preamplifier and feedthroughs, and cryo-cooler. Largest measures in each dimension (mm) are indicated. Note that the flange is ‘squared’. **(b)** Rendering of four Complex detectors tessellated into a wall configuration.

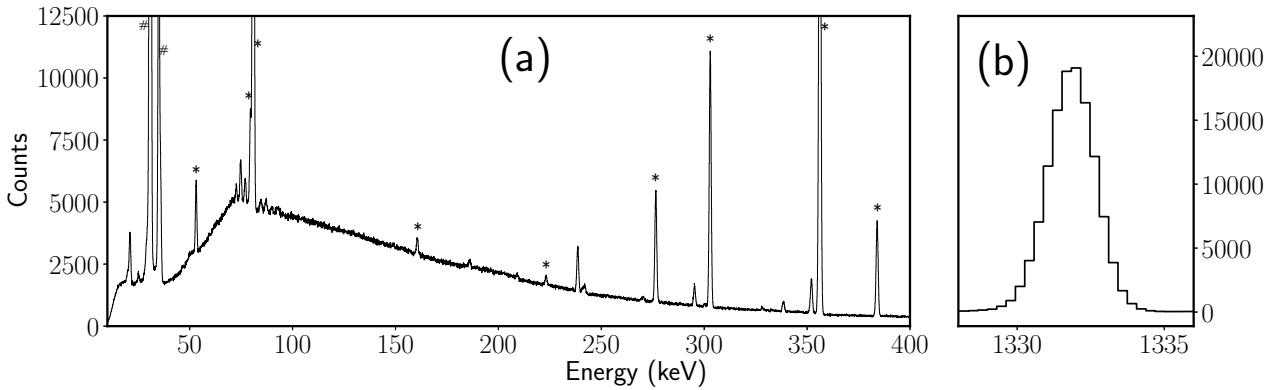


Fig. 3: **(a)** Typical ^{133}Ba spectrum of one Complex crystal. ^{133}Ba γ - and X-ray peaks are indicated with a * and #, respectively. The scale has been set such that the low energy performance is demonstrated. **(b)** Shape of the ^{60}Co 1332 keV peak of one crystal is shown, FWHM = 1.88 keV and FWTM/FWHM = 1.85.

trapezoid and the length of the flat top, respectively, while the decay constant of the preamplifier was 100 μs (changed to 50 μs for final Complex configuration). The digital readout was further processed in line with what has been previously described in Refs. [16,17]. A typical ^{133}Ba spectrum and the ^{60}Co 1332 keV peak of one Complex crystal from these measurements are shown in Fig. 3.

Gaussian peaks convoluted with a linear background were fitted to a region centred around the peak position and if necessary, left tails were included in the fits. The peak properties, centroid, volume and FWHM accompanied with errors were obtained with the program *tv* [18].

3.1 Resolution

A ^{152}Eu source was used in the energy resolution measurements. It was placed centred with respect to the four crystals and at a distance from the end-cap of

the detector such that a count rate of $\sim 1000/\text{s}$ was attained. The duration of each measurement was set such that at least 100 000 counts were accumulated in the peaks of interest.

Figure 4(a) presents the resulting FWHM energy resolution for a single crystal as a function of the peak energy. The function $\text{FWHM}^2 = a + b \cdot E + c \cdot E^2$ was fitted to the data points. The energy resolution is affected by a number of parameters such as leakage current, detector capacitance, charge collection, trapping of charges, operational temperature and noise filter of the amplifier, microphonics *etc.* The measurements with analogue electronics (*cf.* Table 1(a)) and 4 μs shaping time were optimised for best energy resolution at low γ -energies while with digital electronics an enhanced energy resolution of 1.85 keV at 1.33 MeV could be achieved because of the better ballistic deficit correction (see. Fig. 4(a)).

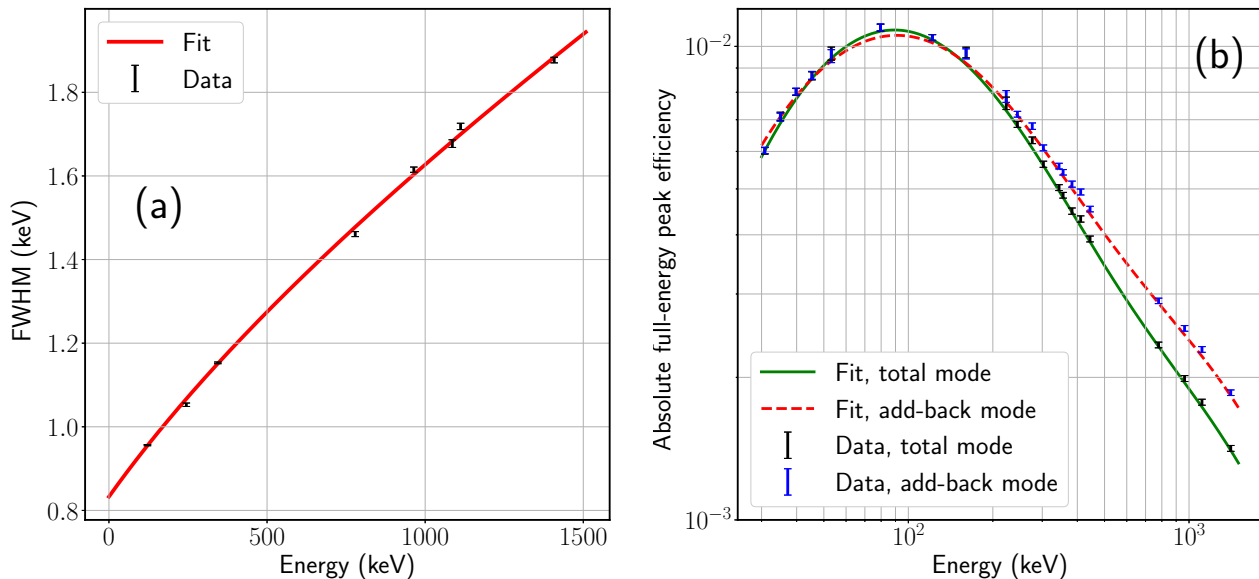


Fig. 4: (a) FWHM energy resolution as a function of peak energy for the direct detection mode. (b) Absolute full-energy peak efficiency at 25 cm distance from source to detector end-cap as a function of peak energy for the total and add-back modes of detection.

3.2 Efficiency

Full-energy peak efficiency of the Compex detector was determined with the so-called external trigger method. A standard $7.68 \times 7.68 \text{ cm}^2$ NaI detector was used as a reference detector. A ^{60}Co source was placed on a holder, centred, and at a distance of 25 cm with respect to the Compex end-cap. The absolute full-energy peak efficiency at 1332 keV was extracted as the ratio of the intensity of 1173 and 1332 keV coincidences and the 1173 keV peak in the NaI. The NaI was mounted at an angle of 90° with respect to the Compex detector. By means of a Monte Carlo simulation, a correction factor of 0.937(10) was determined due to the angular correlation of the 1173 and 1332 keV γ rays. The coincidences were examined in a two-dimensional $\gamma - \gamma$ NaI vs germanium energy spectrum. An energy window was set on the 1173 keV peak in the germanium spectrum and the number of counts were determined by fitting a Gaussian to the projected NaI energy spectrum. The selection was performed on the germanium energy spectrum due to its higher energy resolution.

Efficiency has been measured for the Compex detector in three modes: *direct*, *total*, and *add-back*. In the direct mode, each crystal is used as a single separate detector and the efficiency value is given as an average efficiency of the individual crystals. In the total

mode the spectra of the four crystals are added into one spectrum and thus the efficiency is given for the whole detector. In the add-back mode, if the multiplicity of an event is larger than one and the hits are coincident within 100 ns, their energies are added and the efficiency is then given for the whole detector. All triggered hits are part of the add-back and this translates to an energy threshold of about 15 keV. In order to properly add back the energies of different crystals, the Compex detector channels were calibrated with a ^{152}Eu source and a two-split linear function.

Table 1(b) presents efficiency values at 1332 keV in the different detection modes. The efficiency may be compared to the EUROGAM II Clover detectors (diameter 50 mm and length 70 mm) where the relative efficiency at 1332 keV is in direct mode 21.3(6)% per crystal, and in add-back mode 130(4)% [2].

Spectra in total and add-back detection modes were acquired with ^{152}Eu and ^{133}Ba sources at the same position as the ^{60}Co source. Peaks were fitted to lines widely distributed across an energy range of [30,1400] keV. The relative efficiency of each line was obtained by normalising to tabulated intensities [19]. Following this, the function introduced in Ref. [20]: $\ln \varepsilon(E_\gamma) = ((A + B \cdot x + C \cdot x^2)^{-G} + (D + E \cdot y + F \cdot y^2)^{-G})^{-1/G}$, where $x = \ln(E_\gamma/100)$, $y = \ln(E_\gamma/1000)$, and E_γ is in keV, was fitted to the data by means of a weighted least

squares minimisation. The ratio between the ^{133}Ba and the ^{152}Eu data points was an additional free parameter in the least squares fit. Following the fit to the ^{133}Ba and the ^{152}Eu data, the points and the fitted function were normalised to the absolute value at 1332 keV, given in Table 1(b). Figure 4(b) presents the resulting efficiency curve obtained in the total and add-back detection modes. For a relevant comparison, the reader is referred to Fig. 3 in Ref. [2].

4 Scanning

Three different measurements have been undertaken, namely a front-face scan, a coincidence scan, and source measurements to determine distributions of pulse rise times at three different energies.

Two objectives motivated the front-face scan:

- Verify detector crystal geometry in detail.
- Investigation of detection efficiency across the front face of the detector, especially at the corners.

In turn, the characterisation of the response of a detector, in the case of the other two measurements, had the objective of investigating bulk charge transport properties through the crystal volume in order to identify possible regions of incomplete charge collection.

A distorted electric field due to the shape of the crystals in the Compex detectors could lead to increased trapping [12] and as a consequence energy deficit. This is the main motivation to perform the in-depth characterisation. In the characterisation of the pulse-shape response, extreme or deviating values of the rise time are indications of increased trapping. Therefore, the rise time, defined as the time it takes for the pulse to go from 10% to 90% of its amplitude, is considered a central property in the following. In order to conduct the measurements, a scanning system was designed and built.

4.1 Lund Scanning System

Figure 5 illustrates the *Lund Scanning System* and its working principle. An intense *pencil* beam is created with a ^{137}Cs source and a tungsten collimator. The source is collimated through 100 mm tungsten with a 1 mm diameter hole onto the detector. With an activity of ~ 1.2 GBq, the ^{137}Cs source gives a trigger rate of about 1.5 kHz after collimation.

The collimator is moved over a surface (x, y) in an automated and precise manner with two linear units (one on top of the other) which sit on an elevated steel plate, see Fig. 5(a). The linear units are powered by

NEMA 17[®] stepper motors and controlled via a Raspberry PI[®] - Gertbot interface[®]. The 25 kg collimator sits on a stainless steel arm fixed onto the top linear unit. Photo sensor end-stops enable the reset of the collimator position, essential in calibrating the position of the detector and reproducing scans. An opening with dimensions $120 \times 120 \text{ mm}^2$ sets the boundaries for the (x, y) plane that can be scanned.

The position of the collimator determines the (x, y) coordinate of γ -ray interactions in the detector. The z coordinate is determined through a coincidence method, also utilised in the Liverpool scanning system [21]. As illustrated in Fig. 5(b), four horizontal tungsten collimators with a depth of 50 mm surround the detector. From the bottom up these collimators have a thickness of; 19 mm, 13 mm, 13 mm and 19 mm. Two slits, between the first and second, and second and third collimators, are created with 2.0 mm thick aluminium spacers resulting in a distance of 15 mm between the centres of the slits. Thus two z coordinates are obtained for each (x, y) coordinate. Twenty BGO detectors are arranged in two rows of ten in a quarter of a circle outside of the horizontal collimators, see Fig. 5(b). The BGO detectors are mounted on a dedicated 3D-printed frame such that each row is at the height of the center of a slit and only sees the germanium detector through the respective slit. Coincidence events in the germanium detector and the BGO detectors are in this setup ideally limited to $\sim 90^\circ$ Compton scattered γ rays in the germanium detector, see Fig. 5(b). As the deposited energies in such a reaction are well known, it is in this way also possible to obtain the z coordinate for the γ -ray interaction within the germanium detector.

A manually height adjustable table, able to sustain the large load from the tungsten and steel material, serves as the means to adjust the depth of the interaction point in the crystal, *i.e.* the z coordinate in the coincidence method. The z position of the detector was calibrated with a ^{57}Co source. The source was placed such that it only irradiated the germanium detector through one of the slits. By adjusting the height of the table while monitoring the count rate in the 122 keV peak, the top of the germanium crystal was identified. In the case of the Compex coincidence scan, the calibrated value corresponded very well to the schematic of the end-cap (see Fig. 1(a)). In the measurements, the z coordinate was determined through the measurement of the distance from the end-cap to the elevated steel plate with a caliper.

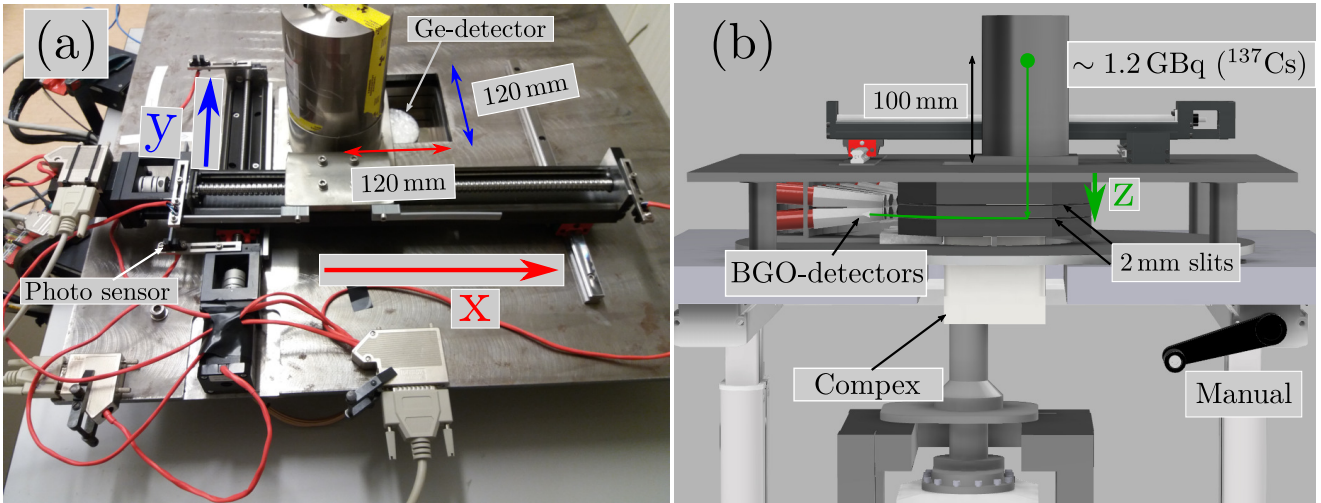


Fig. 5: The Lund scanning system. (a) The system which controls the movement of the collimator, *i.e.* determines the (x, y) -position. (b) The working principle of the coincidence scan method used to determine the z -coordinate. Key measurements and components are indicated.

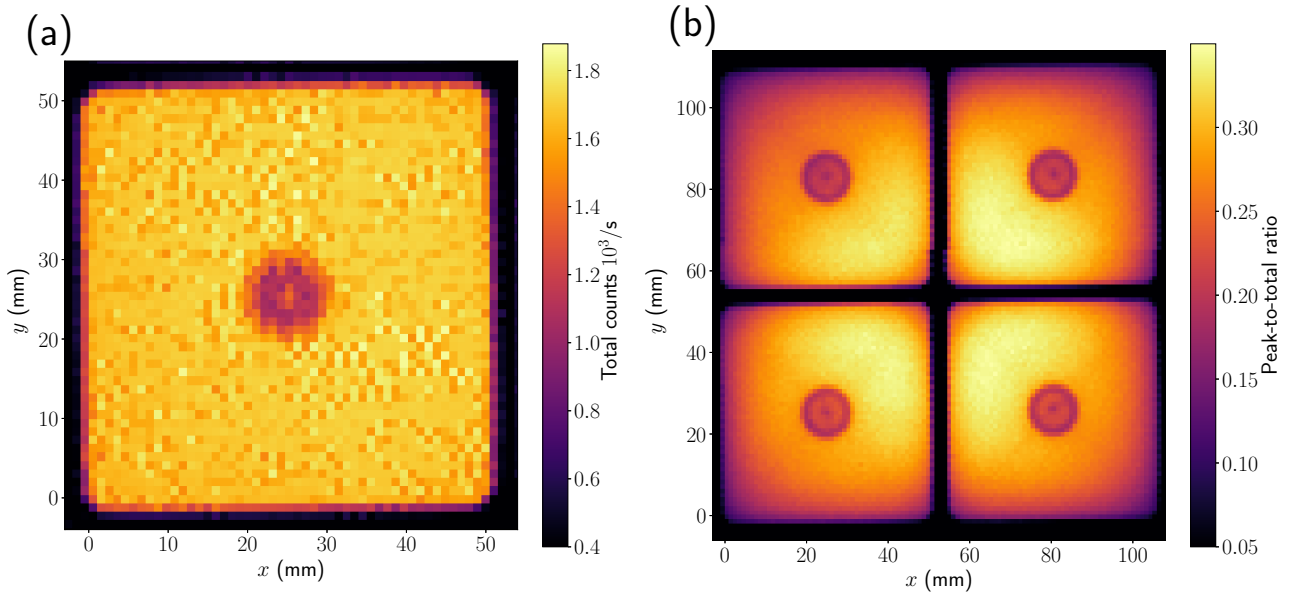


Fig. 6: Front-face scan of the Compex detector obtained with a ^{137}Cs source. (a) The total number of counts below 700 keV per coordinate in direct detection mode for the bottom left crystal. (b) The peak-to-total ratio as a function of position in add-back mode for all four Compex crystals.

4.2 Front-face scan

For the front-face scan, the table was manually adjusted such that the exit of the collimator was sitting at a distance of 15 mm from the front face of the Compex end-cap. The collimator was moved in steps of 1 mm in a grid covering the detector, corresponding to over 13 000 positions. All crystals were set to trigger and data was

collected for 20 s per position and the total number of counts below 700 keV for the ^{137}Cs source was accumulated as a measure of efficiency. Figure 6 shows results from the front-face scan. The total number of counts per second for one crystal in the direct detection mode is presented in Fig. 6(a). The detailed geometry of the crystals, such as a distance of ~ 4 mm between the crystals, and the curved corners, is revealed. The efficiency

shows no degradation as we move from the bore hole towards the sides and the corners of the crystals. At the edges, the decreasing efficiency is caused by the divergence of the pencil beam. Figure 6(b) presents the peak-to-total ratio, defined as the volume of the peak divided by the total counts below 700 keV, per (x, y) coordinate in add-back mode for the four crystals. Here the location of the bore hole and its 10 mm diameter is visible. Due to a larger germanium volume surrounding the corners of the crystals closest to the centre of the detector, the peak-to-total ratio assumes a heterogeneous pattern.

4.3 Coincidence scan

One crystal in a Compex detector was scanned with the coincidence method on a coarser grid. The front-face scan described above together with additional centred-focused front-face scans acted as calibration of the (x, y) position of the crystal. The detector was calibrated with ^{152}Eu source measurements. Signals with $E > 200$ keV in the BGO detectors acted as trigger for the data acquisition, and coincident γ rays in the germanium detector were studied. Traces of 2000 samples were acquired with the SIS3302 100 MHz digitisers. Real coincidences, *i.e.* 90° Compton scatter events in the germanium crystal that is scanned, were extracted based on the following event conditions;

- Multiplicity of one in the BGOs and the germanium crystals
- Germanium energy range of [369, 377] keV
- Time gates, typically 60 ns wide, with respect to trigger, set individually per coordinate

Collections of pulses were in this way extracted for each (x, y, z) -interaction position.

The traces were processed in a similar manner as described in Ref. [21]. Each pulse was interpolated from 10 ns per sample to 2 ns per sample to ensure accurate time alignment. This procedure comprised a five-point linear interpolation followed by a three-point forward moving average. The pulse amplitudes were determined with a moving window deconvolution routine. The pulses were aligned with respect to 10% of its amplitude, denoted T_{10} , while T_{90} was also determined.

Average rise times, defined as $T_{90} - T_{10}$, were extracted for each of the studied interaction positions in the coincidence scan. They are presented in Fig. 7. Measurements of typically 3 h were undertaken per coordinate. This resulted in coincidence yields per coordinate varying from 10 to 100 counts depending on the distance of germanium material the scattered γ ray had to traverse to reach the BGO detectors. In general, the

further the interaction position is from the bore hole, the longer the charge collection path and hence the rise time. Figure 7 shows that this holds for $z = 18$ mm, *i.e.* at a depth with the bore hole, but not at the shallow depth $z = 3$ mm. For $z = 3$ mm, the rise times for the coordinates at the sides are longer compared to the corners, despite shorter charge collection path. The orientation of the fast crystallographic axis along the diagonal of the crystal is a likely explanation to this result [12]. Average pulses for the coordinates along the outer edge for $z = 3$ mm are presented in Fig. 8(a). They also show that the rise times at the sides are longer compared to the corners.

4.4 Pulse shape distributions at three energies

To further investigate pulse shapes, rise time distributions were obtained for ^{241}Am , ^{57}Co , and ^{60}Co sources. The sources were positioned centred with respect to the end-cap such that a count rate of maximum 1 kHz was obtained. Distributions were extracted for the 60, 122, and 1332 keV peaks for one crystal and these are presented in Fig. 8(b). The peak volume, which was at least 40 000 counts, was used in a normalisation. The lower the energy of the γ ray, one expects shallower interaction depths. Generally, the shallower interaction depth, the longer charge collection path and therefore also longer rise times. This is indeed reflected in Fig. 8(b) as the mean rise time shifts to the right with decreasing γ -ray energy. The distributions cover a range of $\sim [50, 250]$ ns of rise times which was probed to a large extent in the (x, y, z) -coincidence scan. Furthermore, the rise times are comparable to the range $\sim [100, 350]$ ns presented for an AGATA crystal in Ref. [13]. The measured energy as a function of the rise time was also studied for these three sources. No trend indicating incomplete charge collection could be identified.

5 Conclusions & outlook

The state-of-the-art composite Compex germanium detector, which is electrically cooled and comprises four single-encapsulated, cubic-shaped, coaxial crystals, has been characterised. Average crystal FWHM energy resolutions of 0.80 and 1.94 keV at 122 and 1332 keV, respectively, demonstrate Compex's great spectroscopic performance. A new scanning system based on a coincidence method has been constructed in Lund. By means of a front-face scan on a fine (x, y) -grid, the compact geometry of the detector was probed. On a coarser (x, y) -grid, the pulse shape response at one shallow and

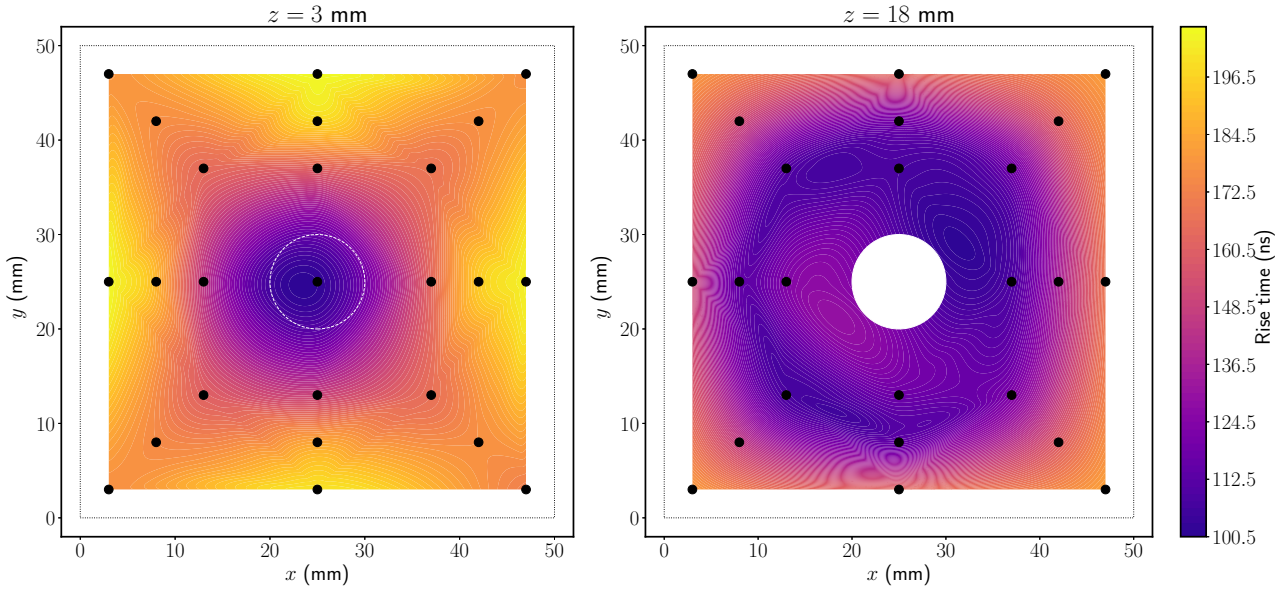


Fig. 7: Average rise times in the coincidence scan for $z = 3$ (left) and $z = 18$ mm (right) illustrated with a cubic interpolation between the data points which are indicated with black filled circles. The bore hole is indicated with a dashed line or filled white circles while the dotted black lines represent the edge of the crystal. For $z = 18$ mm there is no data at the centre since this position is within the bore hole of the crystal.

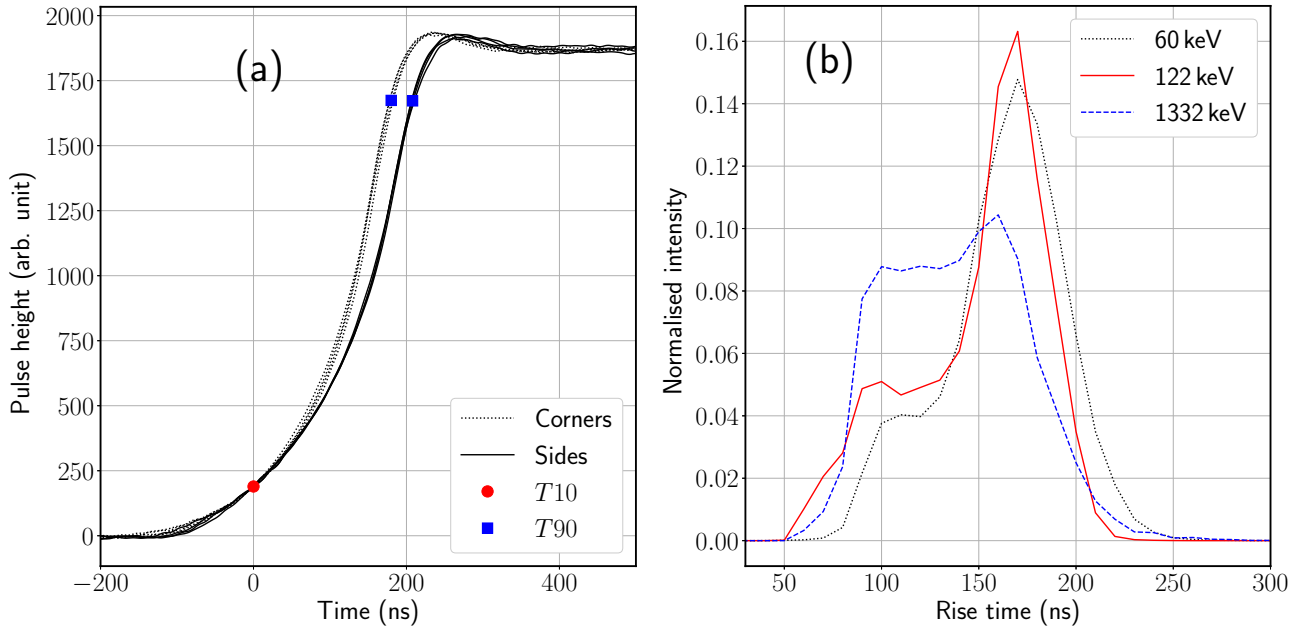


Fig. 8: **(a)** Average pulse shapes along the outer edge at $z = 3$ mm for the four coordinates located at the corner and the side of the crystal, respectively. **(b)** Rise time distributions obtained for ^{241}Am , ^{57}Co , and ^{60}Co sources.

one deeper interaction-depth (z) of one CompeX crystal was investigated in a coincidence scan. These measurements, together with distributions of rise times obtained at three different γ -ray energies, show that the

CompeX detector has pulse shapes typical for that of a coaxial detector with no indications of incomplete charge collection.

The Compex detector, first of its type, opens up the possibility for very high detection efficiencies in decay spectroscopy setups which employ box-shaped vacuum chambers. While four detectors are already a part of the evolved version of TASI Spec [22], with the addition of the fifth electrically segmented Compex detector, the *Lundium* decay spectroscopy setup aims to reach new levels of sensitivity and to push down observational limits for a deeper understanding of the intrinsic structure of nuclei. Future publications and work on the Compex detectors will include characterisations of the electrically segmented Compex detector and the use of all five detectors in the *Lundium* setup. Aided by an improved positional resolution, optimal add-back routines in higher count-rate environments will be a main focus with the segmented Compex detector, while operation without end-caps for increased efficiency at low energy will be one focus in the characterisation of *Lundium*. Finally, in conjunction with Geant4 simulations, the construction of BGO Compton suppression shields for the Compex detectors is underway.

Acknowledgements We would like to thank Gammapool for the use of the EUROBALL inner ball BGO detectors. This work is supported by the Royal Physiographic Society in Lund, and has received funding from the Swedish Research Council (VR 2016-3969), and the Knut & Alice Wallenberg foundation (KAW 2015.0021).

References

1. J. Eberth & J. Simpson, Prog. Part. Nucl. Phys. **60**, 283 (2008).
2. G. Duchêne *et al.*, Nucl. Instrum. Meth. **A 432**, 90 (1999).
3. F.A. Beck, Progress in Particle and Nuclear Physics (1992). Prog. Part. Nucl. Phys. **28**, 443 (1992).
4. J. Eberth *et al.*, Prog. Part. Nucl. Phys. **28**, 495 (1992).
5. J. Eberth *et al.*, Nucl. Instrum. Meth. **A 369**, 135 (1996).
6. J. Simpson, Z. Phys. **A 358**, 139 (1997).
7. G. de France & J. Simpson, Nucl. Phys. News **7**, 12 (2009).
8. S. Akkoyun *et al.*, Nucl. Instrum. Meth. **A 668**, 26 (2012).
9. M.A. Deleplanque *et al.*, Nucl. Instrum. Meth. **A 430**, 292 (1999).
10. L.-L. Andersson *et al.*, Nucl. Instrum. Meth. **A 622**, 164 (2010).
11. D. Rudolph *et al.*, Phys. Rev. Lett. **111**, 112502 (2013).
12. B. Bruyneel, *et al.*, Eur. Phys. J. A **49**, 61 (2013).
13. S.J. Colosimo *et al.*, Nucl. Instrum. Meth. **A 773**, 124 (1995).
14. Cryo-Pulse[®] 5 Plus, Mirion Technologies (Canberra), URL: <https://www.mirion.com/products/cryo-pulse-5-plus-electrically-refrigerated-cryostat>
15. Genie 2000[™], Mirion Technologies (Canberra), URL: <https://www.mirion.com/products/genie-2000-gamma-analysis-software>
16. D. Rudolph *et al.*, Acta Phys. Pol. **B 45**, 263 (2014).
17. Christian Lorenz, PhD thesis, Lund University, ISBN 978-91-7753-943-8 (pdf).
18. J. Theuerkauf, S. Esser, S. Krink, M. Luig, N. Nicolay, O. Stuch, H. Wolters; Program Tv; Institute for Nuclear Physics, Cologne.
19. M.M. Bé, *et al.*, *Table of Radionuclides, Monographie BIPM-5*, vol. 8 (2016).
20. D.C. Radford, Nucl. Instrum. Meth. **A 365**, 297 (1995).
21. M.R. Dimmock *et al.* IEEE Transactions on Nuclear Science **56**, 2415 (2009).
22. D.M. Cox *et al.*, J. Phys. G; Conf. Series, submitted, 2019.